H_2O_2 Photosynthesis from H_2O and O_2 under Weak Light by Carbon Nitrides with Piezoelectric Effect

Jin Ma,[a]‡ Cheng Peng,[b]‡, Xiaoxiao Peng,[a] Sicheng Liang,[a] Zhixin Zhou,[a] Kaiqing Wu,[a] Ran Chen,[a] Songqin Liu,[a] Yanfei Shen,[a] Haibo Ma,[b]* Yuanjian Zhang[a]*

[a] Jiangsu Engineering Laboratory of Smart Carbon-Rich Materials and Device, Jiangsu Province Hi-Tech Key Laboratory for Bio-Medical Research, School of Chemistry and Chemical Engineering, Medical School, Southeast University, Nanjing 211189, China, E-mail: Yuanjian.Zhang@seu.edu.cn

[b] Qingdao Institute for Theoretical and Computational Sciences, Qingdao Institute of Frontier and Interdisciplinary Science, Shandong University, Qingdao 266237, China E-mail: haibo.ma@sdu.edu.cn

‡ J. Ma and C. Peng contributed equally to the work.

Abstract

Driven by the essential need of a green, safe, and low-cost approach to producing H_2O_2, a highly valuable multifunctional chemical, artificial photosynthesis emerges as a promising avenue. However, current catalyst systems remain challenging, due to the need of high-density sunlight, poor selectivity/activity, or/and unfavorable thermodynamics. Here, we reported that an indirect $2e^-$ water oxidation reaction (WOR) in photocatalytic H_2O_2 production was unusually activated by C_5N_2 with piezoelectric effects. Under ultrasonication, C_5N_2 exhibited an overall H_2O_2 photosynthesis rate of 918.4 μM/h and an exceptionally high solar-to-chemical conversion efficiency of 2.6% after calibration under weak light (0.1 sun). Mechanism studies showed the piezoelectric effect of carbon nitride overcame the high uphill thermodynamics of *OH intermediate generation, which opened a new pathway for $2e^-$ WOR, the kinetic limiting step in the overall H_2O_2 production from H_2O and O_2. Benefiting from the high efficiency of photocatalytic H_2O_2 production under weak light, the concept was further successfully adapted to biomedical applications in efficient sono-photo-chemodynamic therapy of tumors.

Introduction

H_2O_2, one of the most valuable multifunctional chemicals with strong oxidation power and high energy density[1-5], is widely used in industrial applications, such as clean fuels, wastewater treatment, cleaning, and organic synthesis[6-11]. As an endogenous long-life reactive oxygen species (ROS), H_2O_2 also participates in biological processes and exerts versatile physiological and pathological functions. Thus, it has also been extensively used in biomedical sensing, disinfection, and cancer photodynamic therapy (PDT)[12-15]. The primary methods for H_2O_2 synthesis encompass the anthraquinone process, electrocatalytic O_2 reduction, and direct H_2-O_2 reaction[16-20]. However, these methods are challenged by high energy consumption, high cost, and/or serious safety issues. Therefore, an innovative, onsite, green, safe, and low-cost H_2O_2 production is imperative desired.

Artificial photocatalysis offers a potential way to drive chemical conversions under very mild conditions[21-26]. Recently, engineering polymeric carbon nitride (pCN)-based photocatalysts has become a promising strategy for overall H_2O_2 production by using water and oxygen as raw materials without any sacrificial agents[27-30]. It involves a $2e^-$ oxygen reduction reaction (ORR, Eq. 1) and a $2e^-$ or $4e^-$ water oxidation reaction (WOR, Eq. 2-5)[31]. Nonetheless, direct $2e^-$ WOR process occurs at higher oxidation potential (+1.76 V vs. NHE, Eq. 3), compared to the $4e^-$ WOR (+1.23 V vs. NHE, Eq. 2). The stepwise $2e^-$ WOR process (Eq. 4-5) requires intermediate hydroxyl radicals (•OH, +2.73 V vs. NHE, Eq. 4), which makes indirect $2e^-$ WOR difficult to occur[32,33]. Therefore, the high uphill thermodynamics of $2e^-$ WOR process significantly limits the overall photocatalytic H_2O_2 production, resulting in a low solar-to-chemical conversion (SCC) efficiency[34-37]. In addition, most photocatalysts work under strong light irradiation in laboratory conditions. It makes practical challenges in photocatalytic H_2O_2 generation in weak light conditions, e.g., under cloudy/overcast circumstances or for deep tissues PDT owing to light scatters[38-41].

$2e^-$ ORR:

$$O_2 + 2H^+ + 2e^- \rightarrow H_2O_2 \qquad 0.69 \text{ V vs. NHE} \qquad (1)$$

$4e^-$ WOR:

$2H_2O + 4h^+ \rightarrow O_2 + 4H^+$ 1.23 V vs. NHE (2)

Direct 2e⁻ WOR:

$2H_2O + 2h^+ \rightarrow H_2O_2 + 2H^+$ 1.76 V vs. NHE (3)

Indirect 2e⁻ WOR:

$H_2O + h^+ \rightarrow \bullet OH + H^+$ 2.73 V vs. NHE (4)

$2\bullet OH \rightarrow H_2O_2$ 1.14 V vs. NHE (5)

Enhancing the adsorption/activation of water and the formation of *OH intermediate is the key rate-determining step for WOR half-reaction[32]. Zare et al. proposed a microdroplet method to prepare H_2O_2, in which an extremely high electric field was formed at the gas-liquid interface of the microdroplet[42,43]. The surface hydroxyl radicals and free electrons were generated at microdroplet interface, which recombined and generated H_2O_2. Similarly, manipulating piezoelectric effect of noncentral symmetric semiconductors induced by mechanical energy can also change both the selectivity and activity of WOR[44-47]. Piezoelectric effect-induced electron hole separation in the polar field would compensate/overcome the thermodynamic potential of WOR to directly generate surface active hydroxyl groups that continue to generate hydrogen peroxide[48]. Nonetheless, despite of the great success of these investigations, the production yield of H_2O_2 remains low.

Herein, we proposed a facile approach for boosting H_2O_2 photosynthesis efficiency from H_2O and O_2 under weak light without any sacrificial agents, relying on piezoelectric-effect of carbon nitrides. Under ultrasonication, electron exchange could occur between pCN and water with repetitive contact and separation cycles at the interface. The H_2O_2 production rate of C_5N_2 reached 918.4 μM/h in weak light (10 mW/cm^2) and 480.1 μM/h in dark without any sacrificial agents or co-catalysts, which exceeded most piezo-photocatalytic processes on carbon nitride and piezo-catalytic processes[46,49-52]. The theoretical calculations further disclosed that ORR and WOR have emerged as appealing processes in the reaction, and both photocatalysis and piezoelectric effect promoted the bond activation and accelerated the generation of *OH species in the indirect two electron WOR, leading to a favorable kinetics and a boosted H_2O_2 production and reaction efficiency. Based on this, C_5N_2 was successfully applied

to sono-photo-chemodynamic therapy (SPCDT) for the first time, demonstrating competitive performances. This work would open a new avenue for highly efficient and selective photosynthesis of H_2O_2, particularly in weak light conditions, and pave their intriguing applications in energy, biomedicine, and environments.

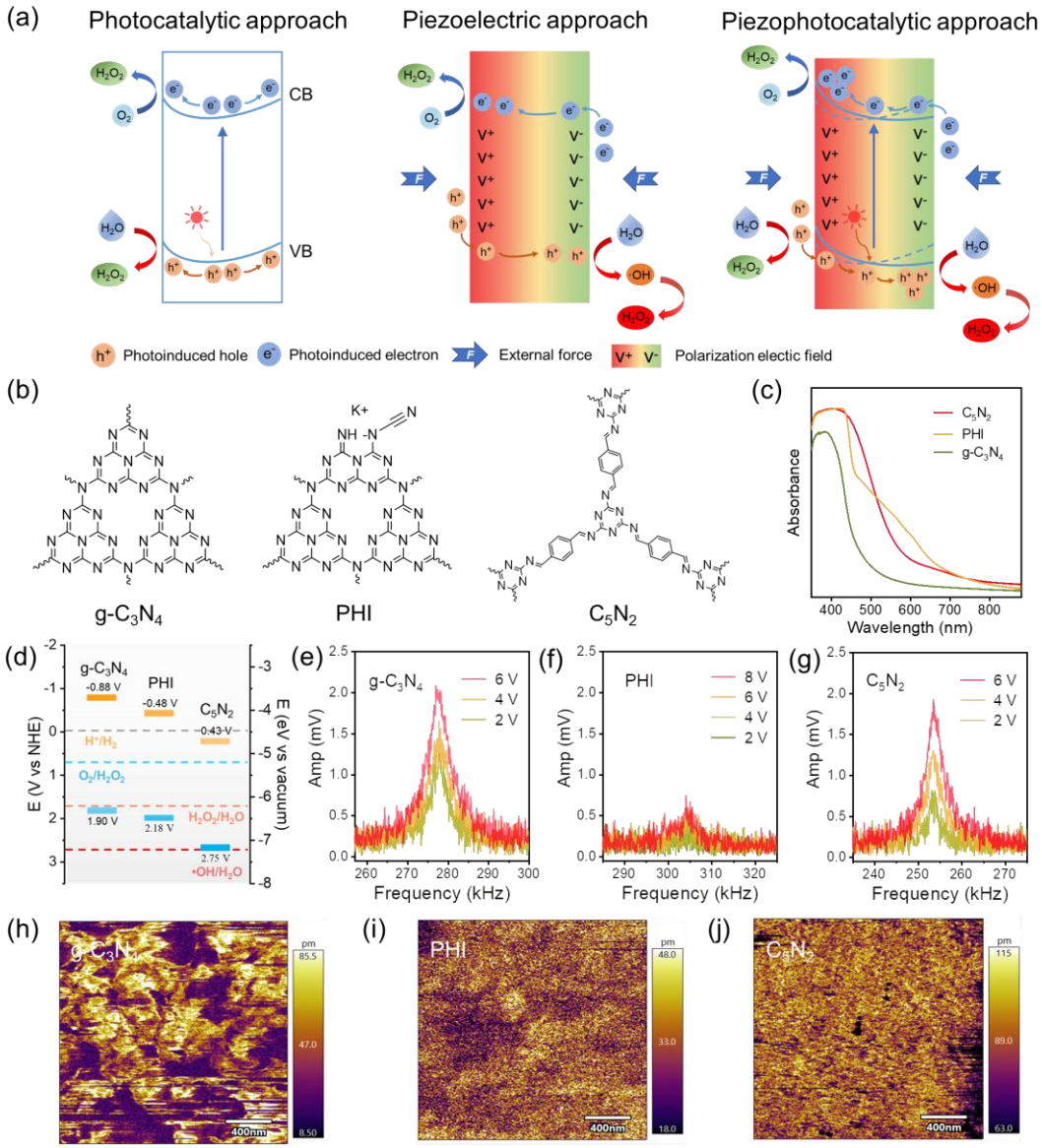

Figure 1. Strategy of piezophotocatalytic H_2O_2 overall production and piezoelectric effects of pCN. (a) Proposed mechanism of the photocatalytic approach, piezoelectric approach, and piezophotocatalytic approach for overall H_2O_2 production. (b) Molecular units, (c) UV-vis diffusion reflection spectra, (d) band positions of g-C_3N_4, PHI, and C_5N_2. Resonant peaks of g-C_3N_4 (e), PHI (f) and C_5N_2 (g) under

different applied voltages, and corresponding PFM amplitude images of g-C_3N_4 (h), PHI (i) and C_5N_2 (j).

Results and discussion

Materials characterization

C_5N_2 was synthesized via a mild liquid Schiff base reaction, and the widely used pCN-based photocatalysts, i.e., g-C_3N_4 and Poly(heptazine imide) (PHI) samples as control samples, were prepared by a conventional thermal polymerization[13,53]. The molecular structure of pCN-based photocatalysts consist of repetitive triazine or heptazine rings units (Fig. 1b). Compared to the idealized g-C_3N_4, C_5N_2 contained a distinct conjugated C=N and benzene linker, and PHI consisted of an incomplete heptazine ring with cyanide terminator (C≡N) (Fig. S1). The microstructure of the samples was investigated using transmission electron microscopy (TEM), and all exhibited a thick layered bulk structure (Fig. S2). The X-ray diffraction (XRD) pattern (Fig. S3) showed two typical diffraction peaks that can be attributed to the (100) and (002) planes of C_5N_2, g-C_3N_4 and PHI, respectively[54]. The UV-visible absorption spectroscopy was used to explore the optical absorption properties (Fig. 1c). Compared to g-C_3N_4, C_5N_2 and PHI showed a redshift absorption edge and tail peak above 460 nm, owing to the enhanced π-electronic transitions in conjugated CN framework and defects, respectively. Likewise, the maximum of photoluminescence wavelength gradually red-shifted (Fig. S4). As calculated by using UV-vis spectra and XPS-VB scan spectra[55], a significant downshift of the CB and VB position of C_5N_2 with respect to g-C_3N_4 and PHI was observed, which indicated the order of the water oxidation ability as C_5N_2 > PHI > g-C_3N_4 (Fig. 1d, Fig. S5).

The unusual piezoelectric properties of g-C_3N_4, PHI and C_5N_2 were further investigated by the piezoresponse force microscopy (PFM). As shown in Figure 1e, three distinct resonant peaks reflecting the piezoelectric vibration excited by voltage in different carbon nitrides were observed. The piezoelectric amplitude of C_5N_2 at the same voltage was comparative to the bulk g-C_3N_4, while that of PHI was weaker. The

amplitude exhibited a significant linear correlation with the excitation voltage (Fig. S6), confirming the linear piezoelectricity of the pCN-based materials[56]. Moreover, the amplitude signals of all the materials were measured in PFM amplitude mapping (Fig. 1f) and the relaxation of the piezoelectric domain polarization were also clearly observed by PFM phase analysis[57]. Besides, the PFM amplitude mapping and phase mapping were entirely consistent with the topography, indicating the uniform distribution of polarization in all materials (Fig. S7). These results demonstrated the presence of piezoelectric response in pCN-based materials, which was supposed to endow pCNs particles with piezocatalytic activity during ultrasonic irradiation[58-60].

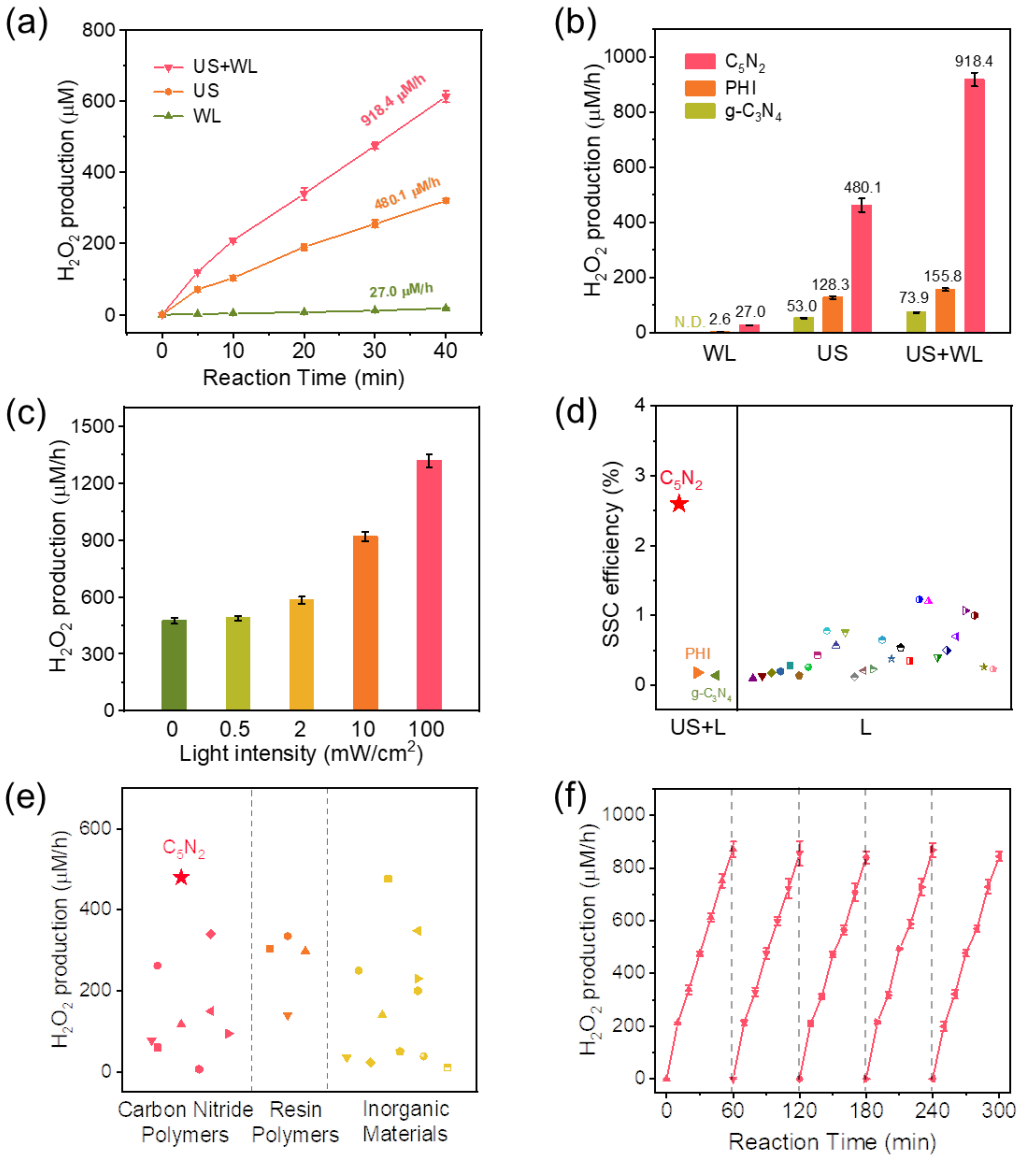

Figure 2. Activity of piezophotocatalytic H_2O_2 production from water and oxygen. (a) Time profiles of H_2O_2 production catalyzed by C_5N_2 in various scenarios. Experimental conditions: 40 mg catalysts in 40 mL of pure water (pH = 7) in an ultrasonic cleaner (US, 40 kHz, 400 W, 100% duty cycle) or/and under weak light (WL, $\lambda > 400$ nm, 10 mW/cm^2) irradiation, T = 25 °C. (b) Contrastive photosynthetic H_2O_2 activity of g-C_3N_4, PHI and C_5N_2 under WL or/and US. Not Detected = N.D. (c) Comparison of H_2O_2 yields by C_5N_2 in different light intensity under US. (d) SCC efficiency of C_5N_2, PHI and g-C_3N_4 (40 mg) in water (40 mL) under WL or/and US, and summarized SCC efficiencies from reported photocatalysts for H_2O_2 production[6,22,29,61-83]. (e) Summary piezoactivity of H_2O_2 production from different reported catalysts under ultrasonication irradiation[45,46,48,52,84-100]. (f) Cycling performance of piezophotocatalytic H_2O_2 production. Error bars represent the standard deviations of three replicate measurements.

Piezoelectric effect in photocatalytic H_2O_2 production.

To investigate the role of piezoelectric effect in photocatalytic H_2O_2 production, C_5N_2, g-C_3N_4 and PHI were placed in a reactor under both ultrasonic (US) force and visible light (L) conditions (Fig. S8). Fig. 2a showed the H_2O_2 generation rates in 40 minutes achieved on C_5N_2 driven by a weak light (WL) in various scenarios, following the order US+WL > US > WL. The piezoelectric effect via ultrasonication improved the H_2O_2 production rate of C_5N_2 to 918.4 μM/h in weak light without any sacrificial agents and co-catalysts, which was a nearly 34 times and 2 times enhancement than that under only weak light and ultrasonication conditions. The photosynthetic H_2O_2 activity of g-C_3N_4 and PHI were also enhanced via the piezoelectric effect (Fig. 2b), reaching 73.9 μM/h and 155.8 μM/h, respectively, but far less than that of C_5N_2. Moreover, g-C_3N_4 and PHI can hardly produce H_2O_2 under weak light irradiation. Fig. 2c showed that piezoelectric effect can enhance the photosynthetic H_2O_2 process under different light intensity, and the H_2O_2 production rate of C_5N_2 can reach 1343.6 μM/h without any sacrificial agents in one sun irradiation (100 mW/cm^2, Fig. S9). The SCC is the

most reliable criterion for photosynthetic H_2O_2 process, which was demonstrated in Fig. 2d. The SCC of C_5N_2 reached 2.6 % (exclude piezocatalysis, see detailed calculation in Table S1) in 10% intensity of one sun (10 mW/cm^2), setting a record in this area[6,22,29,61-83]. Moreover, C_5N_2 also demonstrated by far the highest H_2O_2 piezocatalytic activity (480.1 μM/h) under ultrasonic irradiation among the reported piezocatalysts (Fig 2e, Table S2)[45,46,48,52,84-100]. In addition, the piezophotocatalytic H_2O_2 production rate of C_5N_2 in weak light was well maintained after several repeated cycles, manifesting its excellent stability (Fig. 2f).

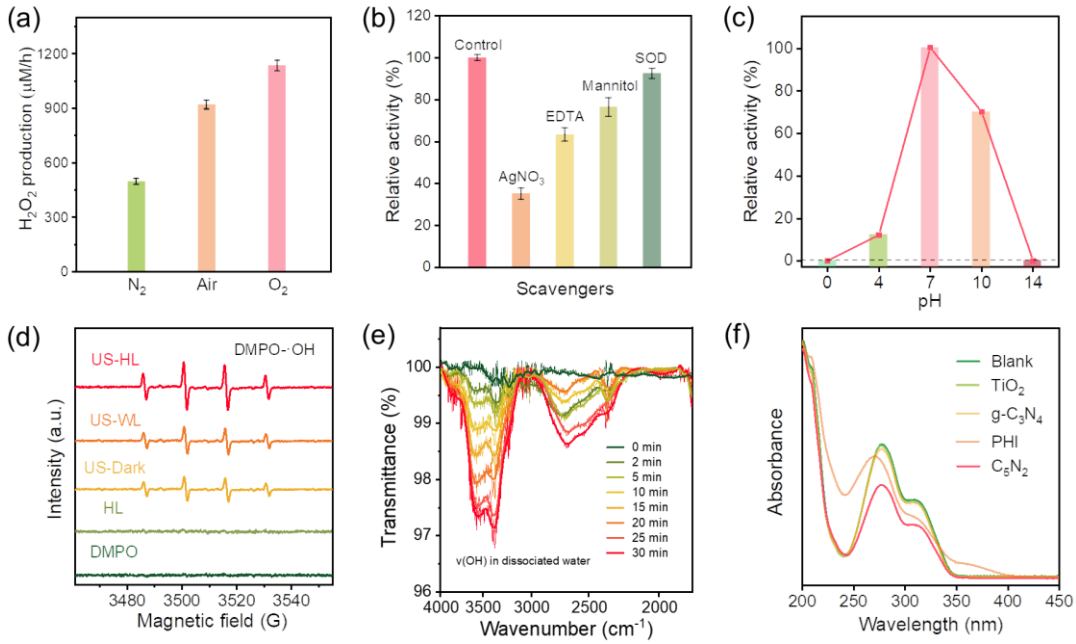

Figure 3. Mechanism of piezophotocatalytic H_2O_2 production. (a) Piezophotocatalytic H_2O_2 production by C_5N_2 in deionized water over different reaction atmospheres. (b) Piezophotocatalytic H_2O_2 production by C_5N_2 in deionized water with different scavengers. (c) Piezophotocatalytic H_2O_2 production by C_5N_2 in deionized water over different pH values. (d) EPR spectra for DMPO-•OH in C_5N_2 aqueous dispersion under ultrasonication (US) or/and various intensities of light (L) irradiation in air atmosphere. (e) In situ FTIR spectra of the H_2O dissociation process over C_5N_2 under ultrasonication and light irradiation. (f) UV-vis absorbance spectra of Cou after reaction with •OH generated by C_5N_2, g-C_3N_4, PHI and TiO_2(P_{25}) before and after ultrasonication and weak light irradiation.

General charge migration behaviors in photocatalytic H_2O_2 production

Compared with g-C_3N_4 and PHI, the higher performance of C_5N_2 for H_2O_2 production under ultrasonication and weak light suggested the enhanced activity and selectivity of half-reactions during the catalytic process. To identify the mechanisms in H_2O_2 production, WOR and ORR processes were investigated separately to understand insights into the exceptionally high efficiency of piezophotocatalytic H_2O_2 production. For this purpose, the aqueous solutions containing different concentrations of dissolved molecular oxygen were firstly explored. Fig. 3a showed the H_2O_2 production efficiency of C_5N_2 was relatively higher in the presence of O_2 during the reaction as well as kept nearly half of that in the O_2-saturated one, suggesting an ORR and WOR mode under weak light and ultrasonication[101]. In this case, when $2e^-$ ORR was inhibited under hypoxic conditions, the pathway of WOR would still work for H_2O_2 production.

Next, trapping experiments were performed to further examine the types of as-produced radicals. The scavengers used were mannitol for •OH, SOD for superoxide radical ($•O_2^-$), EDTA for hole, $AgNO_3$ for electron (Fig. 3b, Fig. S10). It was observed that by adding hole and electron scavengers, the H_2O_2 production efficiency of C_5N_2 under US and WL irradiation demonstrated a various degree of significant inhibition, indicating not only ORR but also WOR occurred. Furthermore, after adding $•O_2^-$ and •OH scavengers respectively, the H_2O_2 production efficiency of C_5N_2 under US and WL irradiation exhibited almost unchanged and obvious inhibition. It suggested that one-electron reduction of O_2 to form •OOH could be excluded and one-electron oxidation of H_2O to form •OH should occur.

The H_2O_2 production over C_5N_2 for a wide pH range (pH 0–14) were also explored (Fig. 3c, Fig. S11). Negligible H_2O_2 was observed from the experimental system with high concentration of H^+ or OH^-. It indicated that both high concentration of H^+ or OH^- would affect the ORR and WOR half-reactions, and the optimum pH was at 7, which was essential for biomedical applications.

The intermediates were further characterized during the photocatalytic H_2O_2 production process via C_5N_2 with ultrasonication (Fig. 3d) to get the formation mechanism for H_2O_2. DMPO and TEMP were used to capture the in situ generated $•O_2^-$,

•OH and $^1O_2$, respectively[102,103]. As shown in Fig. 3a, after ultrasonication and weak light were applied, the $•O_2^-$ and $^1O_2$ signals could not be observed, indicating a direct $2e^-$ ORR process in H_2O_2 production (Fig. S12). As the CB position of C_5N_2 was exceptionally lower than the one-electron ORR potential in thermodynamic (−0.33 V vs. NHE), it was reasonable that the one-electron reduction of O_2 to form $•O_2^-$ was excluded. In contrast, an increasing significant characteristic quadruplet peak of DMPO-•OH were observed during ultrasonication and weak light irradiation, while negligible signals were observed from the light irradiation-only experiment. In addition, the ability of •OH generation was correlated to the intensity of light irradiation in the ultrasonication and weak light irradiation conditions (Fig. S10), which trend was similar to the results of H_2O_2 production in adjusting light intensity and ultrasound power (Fig. 2c, Fig. S13).

Isotope experiments were then performed to verify the existence of $2e^-$ WOR for C_5N_2 under ultrasonication and weak light irradiation[13,104,105]. It was supposed that using $H_2{}^{18}O$, $H_2{}^{18}O_2$ would be produced if $2e^-$ photocatalytic WOR occurred. However, $H_2{}^{18}O_2$ was unstable and demanding to be detected by mass spectroscopy. To circumvent this problem, a well-known horseradish peroxidase (HRP)-catalyzed oxidation reaction were performed to transfer the ^{18}O atom in $H_2{}^{18}O_2$ into luminol oxide. The liquid chromatography-mass spectra (LC-MS, Fig. S14) of the oxidized luminol demonstrated a normal luminol oxide-^{16}O (m/z: 180) peak and a new luminol oxide-^{18}O (m/z: 182 and 184) peaks, while the control in only light irradiation shown a weak luminol oxide-^{18}O (m/z: 182) peak, confirming the enhancement of the $2e^-$ WOR for C_5N_2 under ultrasonication and weak light irradiation.

This activity enhancement mechanism on C_5N_2 was further studied by in situ FTIR to analysis of the H_2O dissociation process (Fig. 3e) and by Coumarin (Cou) oxidation method to quantify the free intermediate via variation absorbance spectra (Fig. 3f)[77]. Compared to g-C_3N_4 and PHI, the in situ FTIR spectroscopy of C_5N_2 showed a more increased peak between 3400-3600 cm^{-1} with reaction time under simultaneously ultrasonic and light irradiation (Fig. S15). The wavenumber of ~3,630 cm^{-1} was assigned to the stretching vibration of the OH group in water, and a shoulder at a lower

wavenumber of ~3,450 $cm^{-1}$was attributed to the production of *OH intermediate from water dissociation[24]. This indicated that *OH was an important intermediate on the surface of C_5N_2. The UV-vis absorbance variation spectra of Cou showed a similar trend that more cous are consumed in the reaction with C_5N_2 after ultrasonic and light irradiated, indicating that C_5N_2 generated more free hydroxyl radicals (Fig. S16).

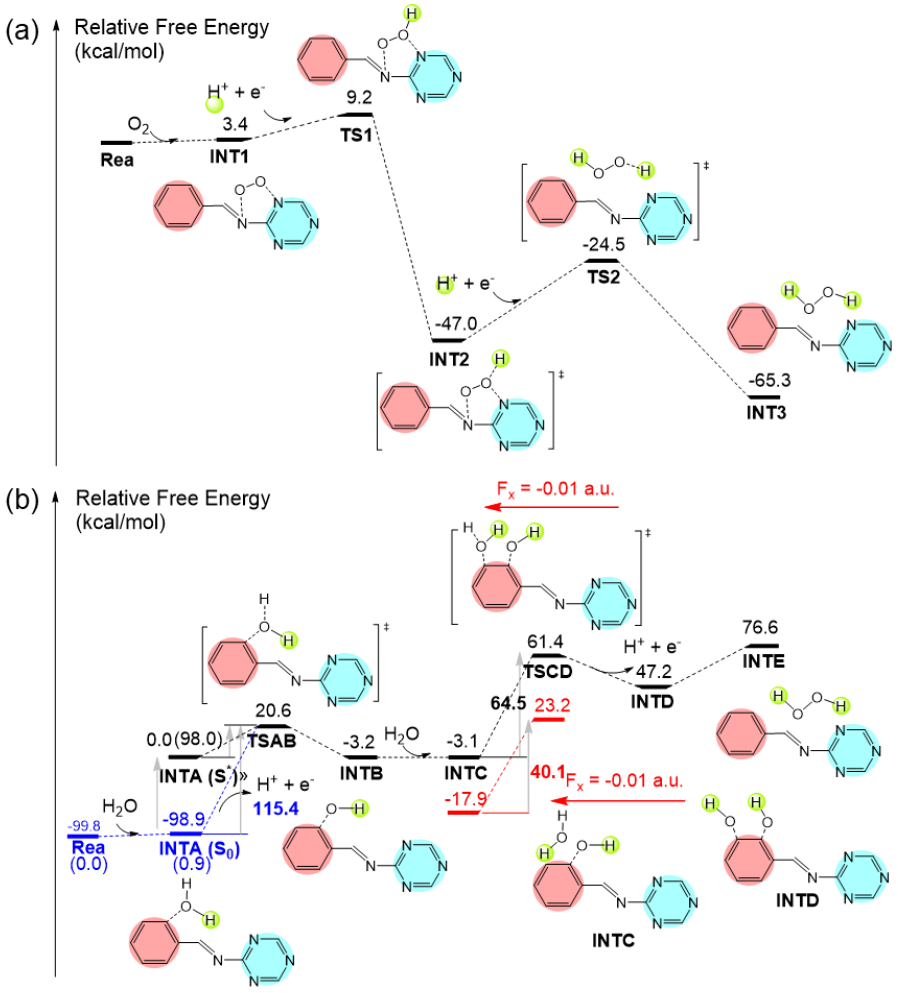

Figure 4. Computational analysis of C_5N_2 in ORR and WOR process. Free energy profile of ORR (a) and WOR with photocatalysis and electric field (b) at the PCM (H_2O)/B3LYP-D3/6-31G(d,p) level (further computational details are given in the supporting information). The free energy of the photoinduced **INTA** is set as zero and energies (**INTC** and **TSCD**) under electric field (F_x = −0.01 a.u, red arrow) are represented in red.

In order to disclose the reaction pathway of the C_5N_2-assisted H_2O_2 generation, density functional theory (DFT) calculation has been carried out and for the sake of

simplicity and saving resource, only one building block of the bulk CN was taken into consideration (see more computational details in SI). As shown in Figure 4a, for ORR, the adsorption configuration of O_2 onto the CN complex surface had been optimized, and the O–N bonding was observed on the NH moieties, which acted as the reaction sites in the ORR. For the consequent O_2 reduction, the activated O_2 molecules would combine with protons in the solution to generate *OOH and *HOOH intermediates and finally the product H_2O_2 can be obtained. The transition state involving the formation of H_2O_2 from *OOH was the rate-determining step in the ORR reaction and the calculated free energy barrier (ΔG) of this step was about 22.5 kcal/mol. The overall ΔG of two electron ORR was −65.3 kcal/mol, indicative of an energy-favorable pathway.

The process of WOR was shown in Figure S17. H_2O molecules were adsorbed and activated on the benzene ring. Such a transformation would be achieved with a Gibbs activation energy value of about 0.9 kcal/mol. Then H_2O would decompose with generating *OH intermediates. However, the calculated ΔG value for the *OH species formation on the benzene ring through **TSAB** (transition state AB) seems thermodynamically unfavorable under the ground state (115.4 kcal/mol).

As the reaction was light-induced, time-dependent DFT (TD-DFT) computational investigation was further carried out (Fig. 4b, Fig. S18), indicating the excitation energy of **INTA** (intermediate A) was as high as ca. 98.0 kcal/mol. The bright state would attain lower excitation energy and the computed activation energy of transition state **TSAB** would decrease to 20.6 kcal/mol, making the following photocatalytic H_2O_2 process possible. Therefore, considering the excitation energy, it was possible for species before **INTA** forming kinetically more stable structures with longer lifetime. The photoinduced states were energetically accessible for performing the subsequent bond activation and initiating thereby *OH generation. However, another **TSCD** (transition state CD) transition state still exhibited a relatively high free energy barrier (64.5 kcal/mol) during the formation of *OH intermediate. Considering the promoting effect of the ultrasonic experimental condition, here an electric field simulating the

piezoelectric effect was applied to give a qualitative analysis on the reaction mechanism (Fig. 4b). Taking account of the electric fields through calculation, when the electric field intensity increases, the ΔG of *OH generation exhibit a tendency to decrease, varying from 64.5 kcal/mol (without electric field) to 61.2 and 41.1 kcal/mol (F_x = –0.005 and –0.01 a.u. respectively, Figure S19). Moreover, when the electric field magnitude increased (F_x = –0.012 and –0.0125 a.u.), the reaction would proceed via a barrierless model. In these regards, the O_2 reduction was thermodynamically more favorable than the water oxidation reaction. It well explained why the two electron WOR limits the photocatalytic efficacy of overall H_2O_2 production. More importantly, the crucial transition state in photocatalytic WOR turns to be more advantageous under external fields, particularly under ultrasonic irradiation to completely break the kinetic limitation, activating the uncommon indirect $2e^-$ WOR pathway (Eq. 4 and 5). These computational findings are not only consistent with the experimental results, but also theoretically prove the high efficiency in the ultrasonic-combined C_5N_2 photocatalytic system. Based on the above experimental and theoretical results, a mechanism of ultrasonic induced WOR to promote photocatalytic synthesis of H_2O_2 over C_5N_2 in the H_2O/O_2 system is proposed in Fig. 5.

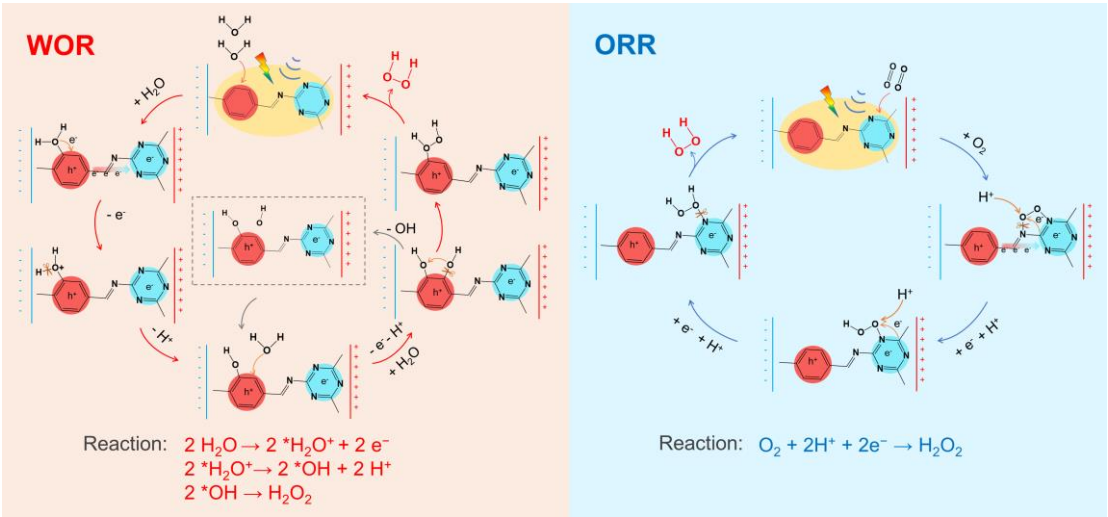

Figure 5. Proposed mechanism of H_2O_2 generation under light and ultrasonic irradiation. Reaction processes and pathways of WOR and ORR on C_5N_2.

Potential application of complementary sono-/photo-/chemo-dynamic therapy (SPCDT)

In conventional cancer therapy, light has been used as a non-invasive therapeutic tool, and photodynamic therapy (PDT) combined light, photosensitizer(s) and molecular dissolved oxygen (O_2) to generate reactive oxygen species that give rise to cellular toxicity[15,106-108]. As another kind of ROS-based therapeutic modality, chemodynamic therapy (CDT) exploits the endogenous stimulus to in situ generate highly harmful •OH from H_2O_2 through an in-situ Fenton or Fenton-like catalytic reaction[109-111]. As two emerging cancer treatments, PDT and CDT still faces two notable limitations. On one hand, PDT suffers from a lower penetration of light into deep tumor sites as light is required for sensitizer activation. On the other hand, hypoxia and insufficient H_2O_2 in cellular environment were unable to provide sufficient original reagents for ROS synthesis, which seriously limit the therapy efficiency[112,113]. By taking advantage of outstanding sonication-assisted photocatalytic H_2O_2 generation under weak light, we sought to adapt the application of C_5N_2 for sono-/photo-/chemo-dynamic cancer treatment to overcome the above issues. To the best of our knowledge, despite great success in non-sacrificial H_2O_2 production, metal-free polymeric photocatalysts have been rarely explored for complementary sono-/photo-/chemo-dynamic cancer treatment to enhance the efficiency.

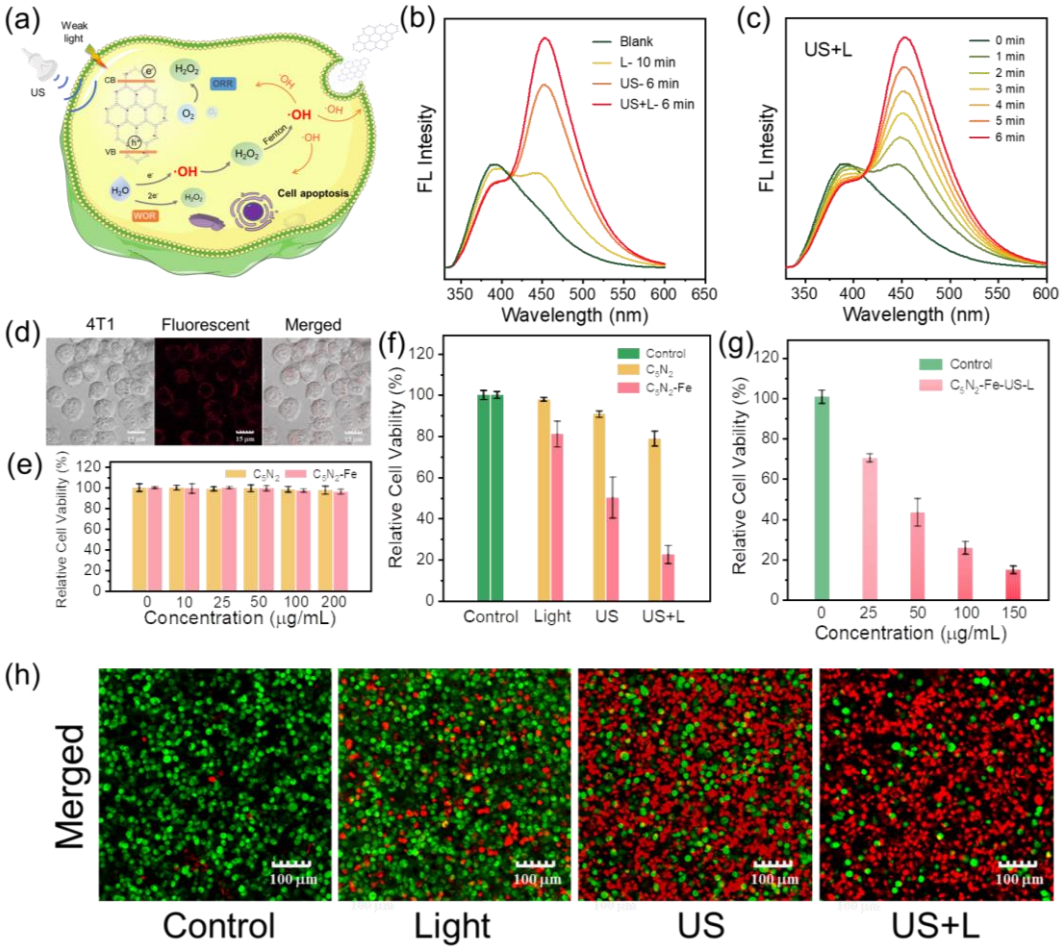

Figure 6. Potential biomedical application of C_5N_2. (a) Scheme of therapeutic processes using C_5N_2 through the Fenton reaction generating •OH under ultrasonic and light irradiation. (b) PL spectra of Cou after reaction with •OH generated by C_5N_2-Fe-NS before and after ultrasonic or/and light irradiated (10 mW/cm^2, λ = 400-900 nm; 1.0 MHz, 1.5 W/cm^2, 6 min, 100% duty cycle). (c) PL spectra of Cou after reaction with •OH generated by C_5N_2-Fe-NS before and after ultrasonic and light irradiated for different time. (d) Confocal fluorescence images of 4T1 cells upon incubation with C_5N_2-Fe-NS. (e) Biocompatibility evaluation of C_5N_2-Fe-NS upon incubation with 4T1 cells by WST-8. (f) Cell viability assay by C_5N_2-Fe-NS and C_5N_2-NS treated 4T1 cells in various scenarios. (g) Cell viability assay by different concentrations of C_5N_2-Fe-NS treated 4T1 cells under ultrasonic and light irradiation. (h) Live/dead double staining of C_5N_2-Fe-NS treated 4T1 cells under ultrasonic and light irradiation indicated by FDA (green, live cells) and PI (red, dead cells).

Controlling intracellular generation of highly toxic •OH via transition metal ion-mediated Fenton or Fenton-like reaction has been reported as an effective antitumor approach to provide direct potent injury to cancer cell[14,111]. We then developed a C_5N_2-based •OH generator and fluorescence agent for complementary sono-/photo/chemo-dynamic tumor therapy (Fig. 5a), which exhibited a competitive tumor inhibition effect. For this, the pristine C_5N_2 was exfoliated into nanosheets and decorated with Fe ions by a ball milling method (C_5N_2-Fe-NS, Fig. S19)[114,115]. After simple separation, the DLS analysis showed that C_5N_2-Fe-NS displayed a narrow size distribution in aqueous solution, with a hydrodynamic size of ~80 nm; the TEM image in Fig. S20 confirmed that C_5N_2-Fe-NS was of layered nanosheets. The production of •OH was verified through the Fenton-like reaction using Cou as a probe. The probe displayed a new fluorescence emission enhancement at 455 nm upon the reaction to •OH. Compared with only light irradiation, the oxidation product of Cou exhibited a gradual amplification of fluorescence intensity with C_5N_2-Fe-NS under both ultrasonic and light irradiation (Fig. 6b). Meanwhile, as metal ions can react with H_2O_2 generated to produce more •OH, C_5N_2-Fe-NS exhibited a higher fluorescence intensity than unmodified C_5N_2-NS (Fig. S21). With increasing the time of ultrasonication and light irradiation, the oxidation product of Cou exhibited a gradual amplification of fluorescence intensity, indicating that the ability of the Fenton-like reaction could be sustainably amplified by ultrasonic and light irradiation with C_5N_2-Fe-NS (Fig. 5c)[15,116].

To investigate the accumulation of the C_5N_2-Fe-NS in tumor cells, 4T1 cells were cultured and incubated with C_5N_2-Fe-NS, and the fluorescence confocal imaging was then measured. As shown in Fig. 6d and Fig. S22, the cytoplasm of the 4T1 cells displayed prominent fluorescence signals in the red channel, leaving the focal nucleus with no fluorescence. This observation indicated that C_5N_2-Fe-NS was internalized into the cells with specific localization in the cytoplasm. The *in vitro* cytotoxicity of C_5N_2-Fe-NS was accessed in 4T1 cells by 2-(2-Methoxy-4-nitrophenyl)-3-(4-nitrophenyl)-5-(2,4-disulfophenyl)-2H-tetrazolium Sodium Salt (CCK-8) assay. As shown in Fig. 6e, no noticeable adverse effects were observed in cells after 24 h, indicating the excellent biocompatibility of C_5N_2-Fe-NS. To corroborate the critical role of ROS in the

therapeutic effect of C_5N_2-Fe-NS, the contribution of SDT/PDT/CDT to total cell death was accessed by carrying out the cell viability under different conditions (Fig. 6f). The cell-killing effect of C_5N_2 or C_5N_2-Fe under ultrasonication and light irradiation (1.0 MHz, 1.0 W/cm^2, 3 min, 50% duty cycle; $\lambda > 400$ nm, 30 mW/cm^2, 3 min) was significantly increased compared to that of alone treatment of only with ultrasonication irradiation (1.0 MHz, 1.0 W/cm^2, 3 min, 50% duty cycle) or light irradiation ($\lambda > 400$ nm, 30 mW/cm^2, 6 min). It was mainly attributed to the fact that the C_5N_2-Fe-NS-induced SDT, PDT and CDT jointly produced more significant •OH to induce apoptosis. Meanwhile, C_5N_2-Fe exhibited a significantly increased cell apoptosis and the cell death rate was proportional to the C_5N_2-Fe concentration (Fig. 6g), which further evidenced the Fenton-like effect of C_5N_2-Fe for •OH generation to induce cell death. Furthermore, fluorescein diacetate (FDA) and propidium iodide (PI) were utilized to stain the live and dead cells, respectively. Live/dead cell staining assay (Fig. 6h, Fig. S23) confirmed a more significant cell death caused by C_5N_2-Fe-NS under both ultrasonication and light irradiation than ultrasonication or light irradiation alone in cell environments, which were both in accordance with the above cell viability data. These results overall pointed out that C_5N_2 as a photocatalysts with piezoelectric effect is promising as a highly effective, multifunctional, and safe sono-photosensitizer for enhanced sono-/photo-/chemo-dynamic therapy. It's worth mentioning that C_5N_2 not only revealed effective in biomedical therapy systems, but also been allowed its use as novel potential solar-based water purification agents which are crucial to achieve water disinfection technology in realistic low density of sunlight environments (Fig. S24-S28).

Conclusion

In summary, we report that external piezoelectric field activated a kinetic limiting step in indirect 2e$^-$ WOR by C_5N_2 during the photocatalytic H_2O_2 production from H_2O and O_2. Compared with conventional carbon nitrides, e.g., g-C_3N_4 and PHI, C_5N_2 with extended conjugation showed a higher photocatalytic H_2O_2 production rate of 918.4 μM/h under weak sunlight and ultrasonic conditions. Remarkably, C_5N_2 achieved a corrected solar-to-chemical conversion efficiency of 2.6% for H_2O_2 synthesis, under

one-tenth the intensity of full sunlight. Both experimental and theoretical results provided evidences for the piezoelectric effect in raising the formation of *OH intermediate and speeding generation of H_2O_2 in WOR process. As a proof-of-concept application, C_5N_2 was successfully applied to sono-photo-chemodynamic therapy, shedding lights on tumor treatment with more penetration depth. The potential for piezoelectric effect of the photocatalytic material will be a primary challenge for the continued development of such technology over long-term operation in energy environmental and biomedical fields.

Reference

1 Volokh, M. & Shalom, M. Light on peroxide. *Nat. Catal.* **4**, 350-351 (2021). https://doi.org:10.1038/s41929-021-00620-2

2 Xia, C., Kim, J. Y. & Wang, H. Recommended practice to report selectivity in electrochemical synthesis of H_2O_2. *Nat. Catal.* **3**, 605-607 (2020). https://doi.org:10.1038/s41929-020-0486-1

3 Gong, M. *et al.* Research Progress of Photocatalytic Sterilization over Semiconductors. *RSC. Adv.* **9**, 19278-19284 (2019). https://doi.org:10.1039/c9ra01826c

4 Wang, Q. *et al.* Metal-Free Photocatalysts for Conversion of H(2) O into Hydrogen Peroxide. *ChemSusChem* **15**, e202201514 (2022). https://doi.org:10.1002/cssc.202201514

5 Freese, T., Meijer, J. T., Feringa, B. L. & Beil, S. B. An organic perspective on photocatalytic production of hydrogen peroxide. *Nat. Catal.* **6**, 553-558 (2023). https://doi.org:10.1038/s41929-023-00980-x

6 Wang, X. *et al.* Ambient Preparation of Benzoxazine-based Phenolic Resins Enables Long-term Sustainable Photosynthesis of Hydrogen Peroxide. *Angew. Chem. Int. Ed.* **62**, e202302829 (2023). https://doi.org:10.1002/anie.202302829

7 Huang, G.-Z. *et al.* On–Off Switching of a Photocatalytic Overall Reaction through Dynamic Spin-State Transition in a Hofmann Clathrate System. *J. Am. Chem. Soc.* **145**, 26863-26870 (2023). https://doi.org:10.1021/jacs.3c09513

8 Zhang, D. *et al.* Photocatalytic Abstraction of Hydrogen Atoms from Water Using Hydroxylated Graphitic Carbon Nitride for Hydrogenative Coupling Reactions. *Angew. Chem. Int. Ed.* **61**, e202204256 (2022). https://doi.org:10.1002/anie.202204256

9 Chen, J., Ma, Q., Yu, Z., Li, M. & Dong, S. Platinum-Gold Alloy Catalyzes the Aerobic Oxidation of Formic Acid for Hydrogen Peroxide Synthesis. *Angew. Chem. Int. Ed.* **61**, e202213930 (2022). https://doi.org:10.1002/anie.202213930

10 Das, P., Roeser, J. & Thomas, A. Solar Light Driven H_2O_2 Production and Selective Oxidations Using a Covalent Organic Framework Photocatalyst Prepared by a Multicomponent Reaction. *Angew. Chem. Int. Ed.* **62**, e202304349 (2023). https://doi.org:10.1002/anie.202304349

11 Li, Q. *et al.* Shear Stress Triggers Ultrathin-Nanosheet Carbon Nitride Assembly for Photocatalytic H_2O_2 Production Coupled with Selective Alcohol Oxidation. *J. Am. Chem. Soc.* **145**, 20837-20848 (2023). https://doi.org:10.1021/jacs.3c05234

12 Richards, T. *et al.* A residue-free approach to water disinfection using catalytic in situ generation of reactive

oxygen species. *Nat. Catal.* **4**, 575-585 (2021). https://doi.org:10.1038/s41929-021-00642-w

13 Ma, J. *et al.* Extended Conjugation Tuning Carbon Nitride for Non-sacrificial H_2O_2 Photosynthesis and Hypoxic Tumor Therapy. *Angew. Chem. Int. Ed.* **61**, e202210856 (2022). https://doi.org:10.1002/anie.202210856

14 Liu, C. *et al.* An open source and reduce expenditure ROS generation strategy for chemodynamic/photodynamic synergistic therapy. *Nat Commun* **11**, 1735 (2020). https://doi.org:10.1038/s41467-020-15591-4

15 Li, P. *et al.* Metal-organic frameworks with photocatalytic bactericidal activity for integrated air cleaning. *Nat Commun* **10**, 2177 (2019). https://doi.org:10.1038/s41467-019-10218-9

16 Yang, S. *et al.* Toward the Decentralized Electrochemical Production of H_2O_2: A Focus on the Catalysis. *ACS Catal.* **8**, 4064-4081 (2018). https://doi.org:10.1021/acscatal.8b00217

17 Yang, H. *et al.* Packing-induced selectivity switching in molecular nanoparticle photocatalysts for hydrogen and hydrogen peroxide production. *Nat. Nanotech.* **18**, 307-315 (2023). https://doi.org:10.1038/s41565-022-01289-9

18 Lu, J. N. *et al.* Synergistic Metal-Nonmetal Active Sites in a Metal-Organic Cage for Efficient Photocatalytic Synthesis of Hydrogen Peroxide in Pure Water. *Angew. Chem. Int. Ed.* **62**, e202308505 (2023). https://doi.org:10.1002/anie.202308505

19 Sun, Y., Han, L. & Strasser, P. A comparative perspective of electrochemical and photochemical approaches for catalytic H_2O_2 production. *Chem. Soc. Rev.* **49**, 6605-6631 (2020). https://doi.org:10.1039/d0cs00458h

20 Zhang, Y. *et al.* H_2O_2 generation from O_2 and H_2O on a near-infrared absorbing porphyrin supramolecular photocatalyst. *Nat. Energy* **8**, 361-371 (2023). https://doi.org:10.1038/s41560-023-01218-7

21 Wang, X. *et al.* A Metal-free Polymeric Photocatalyst for Hydrogen Production from Water under Visible Light. *Nat. Mater.* **8**, 76-80 (2009). https://doi.org:10.1038/nmat2317

22 Shiraishi, Y. *et al.* Resorcinol–formaldehyde Resins as Metal-free Semiconductor Photocatalysts for Solar-to-Hydrogen Peroxide Energy Conversion. *Nat. Mater.* **18**, 985-993 (2019). https://doi.org:10.1038/s41563-019-0398-0

23 Hou, H., Zeng, X. & Zhang, X. Production of Hydrogen Peroxide by Photocatalytic Processes. *Angew. Chem. Int. Ed.* **59**, 17356-17376 (2020). https://doi.org:10.1002/anie.201911609

24 Wang, G., Chen, Z., Wang, T., Wang, D. S. & Mao, J. J. P and Cu Dual Sites on Graphitic Carbon Nitride for Photocatalytic CO_2 Reduction to Hydrocarbon Fuels with High C_2H_6 Evolution. *Angew. Chem. Int. Ed.* **61**, e202210789 (2022). https://doi.org:10.1002/anie.202210789

25 Schultz, D. M. & Yoon, T. P. Solar synthesis: prospects in visible light photocatalysis. *Science* **343**, 1239176 (2014). https://doi.org:10.1126/science.1239176

26 Yu, W. *et al.* Photocatalytic Hydrogen Peroxide Evolution: What is the Most Effective Strategy? *Nano Energy* **104** (2022). https://doi.org:10.1016/j.nanoen.2022.107906

27 Sun, L. *et al.* A Minireview: The Mechanism of H_2O_2 Photoproduction by Graphitic Carbon Nitride. *Adv. Energy Sustain. Research* **4**, 2300090 (2023). https://doi.org:10.1002/aesr.202300090

28 Zhang, Y. *et al.* Molecular Heptazine-Triazine Junction over Carbon Nitride Frameworks for Artificial Photosynthesis of Hydrogen Peroxide. *Adv Mater* **35**, e2306831 (2023). https://doi.org:10.1002/adma.202306831

29 Zhang, X. *et al.* Unraveling the Dual Defect Sites in Graphite Carbon Nitride for Ultra-high Photocatalytic H_2O_2 Evolution. *Energy Environ. Sci.* **15**, 830-842 (2022). https://doi.org:10.1039/d1ee02369a

30 Kofuji, Y. *et al.* Carbon Nitride–Aromatic Diimide–Graphene Nanohybrids: Metal-Free Photocatalysts for

Solar-to-Hydrogen Peroxide Energy Conversion with 0.2% Efficiency. *J. Am. Chem. Soc.* **138**, 10019-10025 (2016). https://doi.org:10.1021/jacs.6b05806

31 Cheng, H., Cheng, J., Wang, L. & Xu, H. Reaction Pathways toward Sustainable Photosynthesis of Hydrogen Peroxide by Polymer Photocatalysts. *Chem. Mater.* **34**, 4259-4273 (2022). https://doi.org:10.1021/acs.chemmater.2c00936

32 Hu, X. *et al.* Engineering Nonprecious Metal Oxides Electrocatalysts for Two-Electron Water Oxidation to H_2O_2. *Ad. Energy Mater.* **12**, 2201466 (2022). https://doi.org:10.1002/aenm.202201466

33 Chen, D. *et al.* Covalent Organic Frameworks Containing Dual O_2 Reduction Centers for Overall Photosynthetic Hydrogen Peroxide Production. *Angew. Chem. Int. Ed.* **62**, e202217479 (2023). https://doi.org:10.1002/anie.202217479

34 Ren, P. *et al.* An Atomically Dispersed Mn-Photocatalyst for Generating Hydrogen Peroxide from Seawater via the Water Oxidation Reaction (WOR). *J. Am. Chem. Soc.* **145**, 16584-16596 (2023). https://doi.org:10.1021/jacs.3c03785

35 Tan, H. *et al.* Photocatalysis of water into hydrogen peroxide over an atomic Ga-N_5 site. *Nature Synthesis* **2**, 557-563 (2023). https://doi.org:10.1038/s44160-023-00272-z

36 Cheng, H. *et al.* Rational Design of Covalent Heptazine Frameworks with Spatially Separated Redox Centers for High-Efficiency Photocatalytic Hydrogen Peroxide Production. *Adv. Mater.* **34**, e2107480 (2022). https://doi.org:10.1002/adma.202107480

37 Yue, J. Y. *et al.* Thiophene-Containing Covalent Organic Frameworks for Overall Photocatalytic H_2O_2 Synthesis in Water and Seawater. *Angew. Chem. Int. Ed.* **62**, e202309624 (2023). https://doi.org:10.1002/anie.202309624

38 Yoon, T. P., Ischay, M. A. & Du, J. Visible light photocatalysis as a greener approach to photochemical synthesis. *Nat. Chem.* **2**, 527-532 (2010). https://doi.org:10.1038/nchem.687

39 Zhang, Y. Y. *et al.* Polyurethane sponge assisted recoverable photocatalyst for outdoor weak sunlight-driven efficient water purification. *Appl. Surface Sci.* **638**, 158091 (2023). https://doi.org:10.1016/j.apsusc.2023.158091

40 Song, C. *et al.* Atomically dispersed Ni catalyst to boost weak sunlight-driven CO_2 hydrogenation with 100% CO selectivity. *Appl. Surface Sci.* **609**, 155339 (2023). https://doi.org:10.1016/j.apsusc.2022.155339

41 Harada, N., Sasaki, Y., Hosoyamada, M., Kimizuka, N. & Yanai, N. Discovery of Key TIPS-Naphthalene for Efficient Visible-to-UV Photon Upconversion under Sunlight and Room Light**. *Angew. Chem. Int. Ed.* **133**, 144-149 (2020). https://doi.org:10.1002/ange.202012419

42 Lee, J. K. *et al.* Condensing water vapor to droplets generates hydrogen peroxide. *Proc. Natl. Acad. Sci. USA* **117**, 30934-30941 (2020). https://doi.org:10.1073/pnas.2020158117

43 Chen, B. *et al.* Water-solid contact electrification causes hydrogen peroxide production from hydroxyl radical recombination in sprayed microdroplets. *Proc. Natl. Acad. Sci. USA* **119**, e2209056119 (2022). https://doi.org:10.1073/pnas.2209056119

44 Zhou, X. F., Shen, B., Zhai, J. W. & Hedin, N. Reactive Oxygenated Species Generated on Iodide-Doped $BiVO_4/BaTiO_3$ Heterostructures with Ag/Cu Nanoparticles by Coupled Piezophototronic Effect and Plasmonic Excitation. *Adv. Funct. Mater.* **31**, 202009594 (2021). https://doi.org:10.1002/adfm.202009594

45 Hu, C. *et al.* Orthogonal Charge Transfer by Precise Positioning of Silver Single Atoms and Clusters on Carbon Nitride for Efficient Piezocatalytic Pure Water Splitting. *Angew. Chem. Int. Ed.* **61**, e202212397 (2022). https://doi.org:10.1002/anie.202212397

46 Zhao, J. W. *et al.* Contact-electro-catalysis for Direct Synthesis of H_2O_2 under Ambient Conditions. *Angew. Chem. Int. Ed.* **62** (2023). https://doi.org:10.1002/anie.202300604

47 Pan, L. *et al.* Advances in Piezo-Phototronic Effect Enhanced Photocatalysis and Photoelectrocatalysis. *Adv. Energy Mater.* **10** (2020). https://doi.org:ARTN 2000214 10.1002/aenm.202000214

48 Hu, C. *et al.* Exceptional Cocatalyst-Free Photo-Enhanced Piezocatalytic Hydrogen Evolution of Carbon Nitride Nanosheets from Strong In-Plane Polarization. *Adv. Mater.* **33**, e2101751 (2021). https://doi.org:10.1002/adma.202101751

49 Zhang, X. *et al.* Developing Ni single-atom sites in carbon nitride for efficient photocatalytic H_2O_2 production. *Nat Commun* **14**, 7115 (2023). https://doi.org:10.1038/s41467-023-42887-y

50 Liu, F. *et al.* Covalent organic frameworks for direct photosynthesis of hydrogen peroxide from water, air and sunlight. *Nat Commun* **14**, 4344 (2023). https://doi.org:10.1038/s41467-023-40007-4

51 Fu, M. *et al.* Promoting Piezocatalytic H_2O_2 Production in Pure Water by Loading Metal-Organic Cage-Modified Gold Nanoparticles on Graphitic Carbon Nitride. *Angew. Chem. Int. Ed.*, e202316346 (2023). https://doi.org:10.1002/anie.202316346

52 Wong, K. T. *et al.* Interfacial Schottky junctions modulated by photo-piezoelectric band bending to govern charge carrier migration for selective H_2O_2 generation. *Appl. Catal. B Environ.* **315**, 121581 (2022). https://doi.org:10.1016/j.apcatb.2022.121581

53 Lotsch, B. V. & Schnick, W. From Triazines to Heptazines: Novel Nonmetal Tricyanomelaminates as Precursors for Graphitic Carbon Nitride Materials. *Chem. Mater.* **18**, 1891-1900 (2006). https://doi.org:10.1021/cm052342f

54 Wang, X. *et al.* A Metal-free Polymeric Photocatalyst for Hydrogen Production from Water under Visible Light. *Nat. Mater.* **8**, 76-80 (2008). https://doi.org:10.1038/nmat2317

55 Huang, C. *et al.* Unraveling Fundamental Active Units in Carbon Nitride for Photocatalytic Oxidation Reactions. *Nat. Commun.* **12**, 320 (2021). https://doi.org:10.1038/s41467-020-20521-5

56 Zelisko, M. *et al.* Anomalous piezoelectricity in two-dimensional graphene nitride nanosheets. *Nat. Commun.* **5**, 4284 (2014). https://doi.org:10.1038/ncomms5284

57 Wang, P., Fan, S., Li, X., Duan, J. & Zhang, D. Modulating the Molecular Structure of Graphitic Carbon Nitride for Identifying the Impact of the Piezoelectric Effect on Photocatalytic H_2O_2 Production. *ACS Catal.* **13**, 9515-9523 (2023). https://doi.org:10.1021/acscatal.3c02565

58 Wang, Y. *et al.* Realizing a Strong Visible-light Absorption Band in Piezoelectric 2D Carbon Nitride Sheets for Enhanced Piezocatalysis. *Nano Energy* **104**, 107983 (2022). https://doi.org:10.1016/j.nanoen.2022.107983

59 Wang, Y. *et al.* Ultrasonic activation of inert poly(tetrafluoroethylene) enables piezocatalytic generation of reactive oxygen species. *Nat. Commun.* **12**, 3508 (2021). https://doi.org:10.1038/s41467-021-23921-3

60 Wang, R.-C., Lin, Y.-C., Chen, H.-C. & Lin, W.-Y. Energy Harvesting From g-C_3N_4 Piezoelectric Nanogenerators. *Nano Energy* **83**, 105743 (2021). https://doi.org:10.1016/j.nanoen.2021.105743

61 Shiraishi, Y. *et al.* Sunlight-Driven Hydrogen Peroxide Production from Water and Molecular Oxygen by Metal-Free Photocatalysts. *Angew. Chem. Int. Ed.* **53**, 13454-13459 (2014). https://doi.org:10.1002/anie.201407938

62 Kofuji, Y. *et al.* Graphitic Carbon Nitride Doped with Biphenyl Diimide: Efficient Photocatalyst for Hydrogen Peroxide Production from Water and Molecular Oxygen by Sunlight. *ACS Catal.* **6**, 7021-7029 (2016). https://doi.org:10.1021/acscatal.6b02367

63 Kofuji, Y. *et al.* Mellitic Triimide-Doped Carbon Nitride as Sunlight-Driven Photocatalysts for Hydrogen Peroxide Production. *ACS Sustain. Chem. Eng.* **5**, 6478-6485 (2017). https://doi.org:10.1021/acssuschemeng.7b00575

64 Kofuji, Y. *et al.* Carbon Nitride–Aromatic Diimide–Graphene Nanohybrids: Metal-Free Photocatalysts for Solar-to-Hydrogen Peroxide Energy Conversion with 0.2% Efficiency. *J. Am. Chem. Soc.* **138**, 10019-10025 (2016). https://doi.org:10.1021/jacs.6b05806

65 Kofuji, Y. *et al.* Hydrogen Peroxide Production on a Carbon Nitride–Boron Nitride-Reduced Graphene Oxide Hybrid Photocatalyst under Visible Light. *ChemCatChem* **10**, 2070-2077 (2018). https://doi.org:10.1002/cctc.201701683

66 Chen, L. *et al.* Acetylene and Diacetylene Functionalized Covalent Triazine Frameworks as Metal-Free Photocatalysts for Hydrogen Peroxide Production: A New Two-Electron Water Oxidation Pathway. *Adv. Mater.* **32**, 1521-4095 (2019). https://doi.org:10.1002/adma.201904433

67 Zhu, Z., Pan, H., Murugananthan, M., Gong, J. & Zhang, Y. Visible Light-driven Photocatalytically Active g-C_3N_4 Material for Enhanced Generation of H_2O_2. *Appl Catal B Environ* **232**, 19-25 (2018). https://doi.org:10.1016/j.apcatb.2018.03.035

68 Cao, J. *et al.* Phosphorus-doped Porous Carbon Nitride for Efficient Sole Production of Hydrogen Peroxide via Photocatalytic Water Splitting with a Two-Channel Pathway. *J. Mater. Chem. A* **8**, 3701-3707 (2020). https://doi.org:10.1039/c9ta13929j

69 Cheng, H. *et al.* Rational Design of Covalent Heptazine Frameworks with Spatially Separated Redox Centers for High-Efficiency Photocatalytic Hydrogen Peroxide Production. *Adv. Mater.* **34**, 1521-4095 (2021). https://doi.org:10.1002/adma.202107480

70 Kou, M. *et al.* Molecularly Engineered Covalent Organic Frameworks for Hydrogen Peroxide Photosynthesis. *Angew. Chem. Int. Ed.* **61**, 1521-3773 (2022). https://doi.org:10.1002/anie.202200413

71 Li, L., Xu, L., Hu, Z. & Yu, J. C. Enhanced Mass Transfer of Oxygen through a Gas–Liquid–Solid Interface for Photocatalytic Hydrogen Peroxide Production. *Adv. Funct. Mater.* **31**, 1616-3028 (2021). https://doi.org:10.1002/adfm.202106120

72 Wang, W. *et al.* Visible Light-Induced Marine Bacterial Inactivation in Seawater by an In Situ Photo-Fenton System without Additional Oxidants: Implications for Ballast Water Sterilization. *ACS ES&T Water* **1**, 1483-1494 (2021). https://doi.org:10.1021/acsestwater.1c00048

73 Wu, Q. *et al.* A Metal-free Photocatalyst for Highly Efficient Hydrogen Peroxide Photoproduction in Real Seawater. *Nat. Commun.* **12**, 483 (2021). https://doi.org:10.1038/s41467-020-20823-8

74 Chen, D. *et al.* Covalent Organic Frameworks Containing Dual O_2 Reduction Centers for Overall Photosynthetic Hydrogen Peroxide Production. *Angew. Chem. Int. Ed.* **135**, e202217479 (2023). https://doi.org:10.1002/ange.202217479

75 Yan, H. *et al.* Spontaneous exciton dissociation in organic photocatalyst under ambient conditions for highly efficient synthesis of hydrogen peroxide. *Proc. Natl. Acad. Sci. USA* **119**, e2202913119 (2022). https://doi.org:10.1073/pnas.2202913119

76 Tian, Q. *et al.* Exceptional Photocatalytic Hydrogen Peroxide Production from Sandwich-Structured Graphene Interlayered Phenolic Resins Nanosheets with Mesoporous Channels. *Adv. Funct. Mater.* **33**, 2213173 (2023). https://doi.org:10.1002/adfm.202213173

77 Zhang, Y. *et al.* H_2O_2 generation from O_2 and H_2O on a near-infrared absorbing porphyrin supramolecular photocatalyst. *Nat Energy* **8**, 361-371 (2023). https://doi.org:10.1038/s41560-023-01218-7

78 Tan, H. *et al.* Photocatalysis of water into hydrogen peroxide over an atomic Ga-N_5 site. *Nat. Synth.* **2**, 557-563 (2023). https://doi.org:10.1038/s44160-023-00272-z

79 Tian, Q. *et al.* Nanospatial Charge Modulation of Monodispersed Polymeric Microsphere Photocatalysts for Exceptional Hydrogen Peroxide Production. *Small* **17**, e2103224 (2021). https://doi.org:10.1002/smll.202103224

80 Shiraishi, Y. *et al.* Solar-to-Hydrogen Peroxide Energy Conversion on Resorcinol-Formaldehyde Resin Photocatalysts Prepared by Acid-Catalysed Polycondensation. *Commun. Chem.* **3**, 169 (2020). https://doi.org:10.1038/s42004-020-00421-x

81 Shiraishi, Y., Matsumoto, M., Ichikawa, S., Tanaka, S. & Hirai, T. Polythiophene-Doped Resorcinol–Formaldehyde Resin Photocatalysts for Solar-to-Hydrogen Peroxide Energy Conversion. *J. Am. Chem. Soc.* **143**, 12590-12599 (2021). https://doi.org:10.1021/jacs.1c04622

82 Ye, Y. X. *et al.* A Solar-to-Chemical Conversion Efficiency up to 0.26% Achieved in Ambient Conditions. *Proc. Natl. Acad. Sci. USA* **118**, e2115666118 (2021). https://doi.org:10.1073/pnas.2115666118

83 Liu, L. *et al.* Linear Conjugated Polymers for Solar-Driven Hydrogen Peroxide Production: The Importance of Catalyst Stability. *J. Am. Chem. Soc.* **143**, 19287-19293 (2021). https://doi.org:10.1021/jacs.1c09979

84 Fu, M. *et al.* Promoting Piezocatalytic H_2O_2 Production in Pure Water by Loading Metal-Organic Cage-Modified Gold Nanoparticles on Graphitic Carbon Nitride. *Angew. Chem. Int. Ed.* **63**, e202316346 (2024). https://doi.org:10.1002/anie.202316346

85 Wang, K. *et al.* Enhancing piezocatalytic H_2O_2 production through morphology control of graphitic carbon nitride. *J Colloid Interface Sci* **648**, 242-250 (2023). https://doi.org:10.1016/j.jcis.2023.05.204

86 Wang, K. *et al.* Efficient piezo-catalytic hydrogen peroxide production from water and oxygen over graphitic carbon nitride. *J Mater Chem A* **7**, 20383-20389 (2019). https://doi.org:10.1039/c9ta06251c

87 Tang, R. *et al.* Unique g-C_3N_4/PDI-g-C_3N_4 homojunction with synergistic piezo-photocatalytic effect for aquatic contaminant control and H_2O_2 generation under visible light. *Appl. Catal. B Environ.* **303**, 120929 (2022). https://doi.org:10.1016/j.apcatb.2021.120929

88 Xu, T. T. *et al.* Constructing Crystalline g - C_3N_4/g - C_3N_4−xSx Isotype Heterostructure for Efficient Photocatalytic and Piezocatalytic Performances. *Energy Environ Mater* **6**, e12306 (2023). https://doi.org:10.1002/eem2.12306

89 Fu, C. *et al.* Dual-defect enhanced piezocatalytic performance of C_3N_5 for multifunctional applications. *Appl. Catal. B Environ.* **323**, 122196 (2023). https://doi.org:10.1016/j.apcatb.2022.122196

90 Yin, G. *et al.* Piezocatalytic degradation of organic dyes and production of H_2O_2 with hydroxyapatite. *J Alloys Compd* **937**, 168382 (2023). https://doi.org:10.1016/j.jallcom.2022.168382

91 Zhou, X. *et al.* Efficient Production of Solar Hydrogen Peroxide Using Piezoelectric Polarization and Photoinduced Charge Transfer of Nanopiezoelectrics Sensitized by Carbon Quantum Dots. *Adv. Sci.* **9**, e2105792 (2022). https://doi.org:10.1002/advs.202105792

92 Hu, C. *et al.* Coupling Piezocatalysis and Photocatalysis in Bi_4NbO_8X (X = Cl, Br) Polar Single Crystals. *Adv. Funct. Mater.* **30**, 1908168 (2019). https://doi.org:10.1002/adfm.201908168

93 Ma, Y. *et al.* Bifunctional $RbBiNb_2O_7$/poly(tetrafluoroethylene) for high-efficiency piezocatalytic hydrogen and hydrogen peroxide production from pure water. *Chem. Eng. J.* **446**, 136958 (2022). https://doi.org:10.1016/j.cej.2022.136958

94 Wen, Y. Y. *et al.* Interface Interaction Enhanced Piezo-Catalytic Hydrogen Peroxide Generation via One-Electron Water Oxidation. *Adv. Funct. Mater.* **33**, 2308084 (2023). https://doi.org:10.1002/adfm.202308084

95 Li, Y. *et al.* Robust route to H_2O_2 and H_2 via intermediate water splitting enabled by capitalizing on minimum vanadium-doped piezocatalysts. *Nano Res.* **15**, 7986-7993 (2022). https://doi.org:10.1007/s12274-022-4506-0

96 Jia, Y., Wang, K., Li, C. & Liu, S. Efficient piezocatalytic hydrogen peroxide generation over MAX phase piezocatalysts. *Mater. Today Sustain.* **22**, 100390 (2023). https://doi.org:10.1016/j.mtsust.2023.100390

97 Xu, J. *et al.* Highly Efficient Fe(III) -initiated Self-cycled Fenton System in Piezo-catalytic Process for Organic Pollutants Degradation. *Angew. Chem. Int. Ed.* **62**, e202307018 (2023).

https://doi.org:10.1002/anie.202307018

98 He, J. *et al.* C-Doped $KNbO_3$ single crystals for enhanced piezocatalytic intermediate water splitting. *Environ. Sci. Nano* **9**, 1952-1960 (2022). https://doi.org:10.1039/d2en00244b

99 Zhou, X., Shen, B., Zhai, J. & Hedin, N. Reactive Oxygenated Species Generated on Iodide-Doped $BiVO_4/BaTiO_3$ Heterostructures with Ag/Cu Nanoparticles by Coupled Piezophototronic Effect and Plasmonic Excitation. *Adv. Funct. Mater.* **31**, 202009594 (2021). https://doi.org:10.1002/adfm.202009594

100 Lin, S., Wang, Q., Huang, H. & Zhang, Y. Piezocatalytic and Photocatalytic Hydrogen Peroxide Evolution of Sulfide Solid Solution Nano-Branches from Pure Water and Air. *Small* **18**, e2200914 (2022). https://doi.org:10.1002/smll.202200914

101 Xu, X. *et al.* Conjugated Organic Polymers with Anthraquinone Redox Centers for Efficient Photocatalytic Hydrogen Peroxide Production from Water and Oxygen under Visible Light Irradiation without Any Additives. *ACS Catal.* **12**, 12954-12963 (2022). https://doi.org:10.1021/acscatal.2c04085

102 Hao, F. *et al.* Photo-Driven Quasi-Topological Transformation Exposing Highly Active Nitrogen Cation Sites for Enhanced Photocatalytic H_2O_2 Production. *Angew. Chem. Int. Ed.* **62**, e202315456 (2023). https://doi.org:10.1002/anie.202315456

103 Peng, X. *et al.* Molecular assembly of carbon nitride-based composite membranes for photocatalytic sterilization and wound healing. *Chem. Sci.* **14**, 4319-4327 (2023). https://doi.org:10.1039/d3sc00642e

104 Wu, K. *et al.* Elucidating Electrocatalytic Oxygen Reduction Kinetics via Intermediates by Time-Dependent Electrochemiluminescence. *Angew. Chem. Int. Ed.* **62**, e202217078 (2023). https://doi.org:10.1002/anie.202217078

105 Peng, Y. *et al.* Room-Temperature Synthesized Iron/Cobalt Metal–Organic Framework Nanosheets with Highly Efficient Catalytic Activity toward Luminol Chemiluminescence Reaction. *Anal. Chem.* **95**, 18436-18442 (2023). https://doi.org:10.1021/acs.analchem.3c03538

106 Chen, W. *et al.* A C_5N_2 Nanoparticle Based Direct Nucleus Delivery Platform for Synergistic Cancer Therapy. *Angew. Chem. Int. Ed.* **131**, 6356-6360 (2019). https://doi.org:10.1002/ange.201900884

107 Dewaele, M., Maes, H. & Agostinis, P. ROS-Mediated Mechanisms of Autophagy Stimulation and their Relevance in Cancer Therapy. *Autophagy* **6**, 838-854 (2014). https://doi.org:10.4161/auto.6.7.12113

108 Yang, B., Chen, Y. & Shi, J. Reactive Oxygen Species (ROS)-Based Nanomedicine. *Chem. Rev.* **119**, 4881-4985 (2019). https://doi.org:10.1021/acs.chemrev.8b00626

109 Li, S. L., Jiang, P., Jiang, F. L. & Liu, Y. Recent Advances in Nanomaterial-Based Nanoplatforms for Chemodynamic Cancer Therapy. *Adv. Funct. Mater.* **31**, e2100243 (2021). https://doi.org:ARTN 2100243 10.1002/adfm.202100243

110 Cao, C., Wang, X., Yang, N., Song, X. & Dong, X. Recent Advances of Cancer Chemodynamic Therapy based on Fenton/Fenton-like Chemistry. *Chem Sci.* **13**, 863-889 (2022). https://doi.org:10.1039/d1sc05482a

111 Jia, C., Guo, Y. & Wu, F. G. Chemodynamic Therapy via Fenton and Fenton-Like Nanomaterials: Strategies and Recent Advances. *Small* **18**, e2103868 (2021). https://doi.org:10.1002/smll.202103868

112 Zhao, X., Liu, J., Fan, J., Chao, H. & Peng, X. Recent Progress in Photosensitizers for Overcoming the Challenges of Photodynamic Therapy: from Molecular Design to Application. *Chem. Soc. Rev.* **50**, 4185-4219 (2021). https://doi.org:10.1039/d0cs00173b

113 Liu, J.-n., Bu, W. & Shi, J. Chemical Design and Synthesis of Functionalized Probes for Imaging and Treating Tumor Hypoxia. *Chem. Rev.* **117**, 6160-6224 (2017). https://doi.org:10.1021/acs.chemrev.6b00525

114 Han, G.-F. *et al.* Mechanochemistry for ammonia synthesis under mild conditions. *Nat. Nanotech.* **16**, 325-330 (2020). https://doi.org:10.1038/s41565-020-00809-9

115 Ji, J. *et al.* Simultaneous Noncovalent Modification and Exfoliation of 2D Carbon Nitride for Enhanced

Electrochemiluminescent Biosensing. *J. Am. Chem. Soc.* **139**, 11698-11701 (2017). https://doi.org:10.1021/jacs.7b06708

116 Cao, X. *et al.* Insight into Iron Leaching from an Ascorbate-Oxidase-like Fe-N-C Nanozyme and Oxygen Reduction Selectivity. *Angew. Chem. Int. Ed.* **62**, e202302463 (2023). https://doi.org:10.1002/anie.202302463